SITE CHARACTERIZATION REPORT

SLENK: Lenk (BE)

Dario Chieppa, Manuel Hobiger, Donat Fäh

Last Modification: 11th October, 2021

Contents

Summary

Lenk (BE) is a village located at the end of the Simmen valley. The place was chosen as site for the installation of a new station, called SLENK, as part of the renewal project of the Swiss Strong Motion Network (SSMNet). In order to better assess the local subsurface, a passive seismic array with center 50 meters west north-west from the location of station SLENK was performed.

The results of the horizontal-to-vertical spectral ratio (H/V) show several curves with a fundamental H/V peak in a narrow frequency range between 1.4 and 2.0 Hz. The same peak was identified at other sites at lower (down to 1.15 and 1.18 Hz) and higher (2.8 Hz) frequencies. To the right of the H/V peak, a wide trough with amplitudes below 0.2 is recognized at many sites.

The inversion of the passive seismic array measurements allows the estimation of the velocity profiles down to 400 m. Three main interfaces are distinguished at about 11, 32 and 200 meters using velocity profiles with 5, 7, 9 or 11 layers over the half-space and a velocity inversion in the shallow layers. The depth of the basement, as estimated by the best velocity model with nine layers, is located at about 330 m with S-wave velocity of around 1500 m/s.

The V_{S30} value of the site is 175.57 m/s, corresponding to soil class D in EC8 and SIA261. The theoretical shear-wave transfer functions from the retrieved V_S profiles predict an amplification up to 8.7 at 1.7 Hz in good agreement with the empirical function recorded at station SLENK.

1 Introduction

The station SLENK is part of the Swiss Strong Motion Network (SSMNet). The station has been installed on 8 August 2019 in the framework of the second phase of the Swiss Strong Motion Network (SSMNet) renewal project (Fig. 1). In order to better characterize the underground, to estimate the fundamental frequency of the site and the shear wave velocity, a passive array measurement was carried out on 1 October 2020.

The site is of interest for its proximity with the school and for the possibility to improve the network coverage of central Switzerland. From a geological point of view, Lenk is located on undifferentiated alluvial sediments of Holocene age overlying the allochthone Schuppenzone.
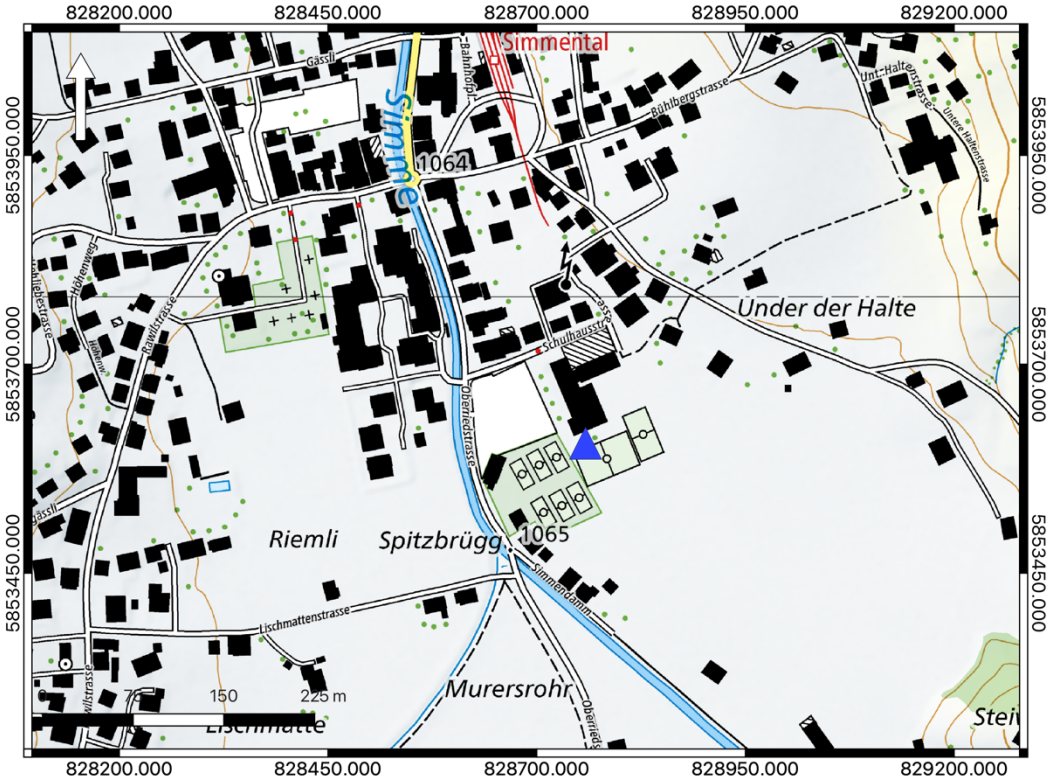

Figure 1: Map showing the location of the strong motion station (blue triangle) in Lenk. Source: Federal Office of Topography.

2 Geological setting

A geological map of the surroundings of Lenk is shown in Fig. 2. Red dots represent the location of the passive array measurement, the blue triangle the location of station SLENK. Most of the installed sensors are located on undifferentiated alluvial sediments (Quaternary) and alluvial fan deposits (Holocene age). The westernmost sensor lies on moraine deposits also of Quaternary age.
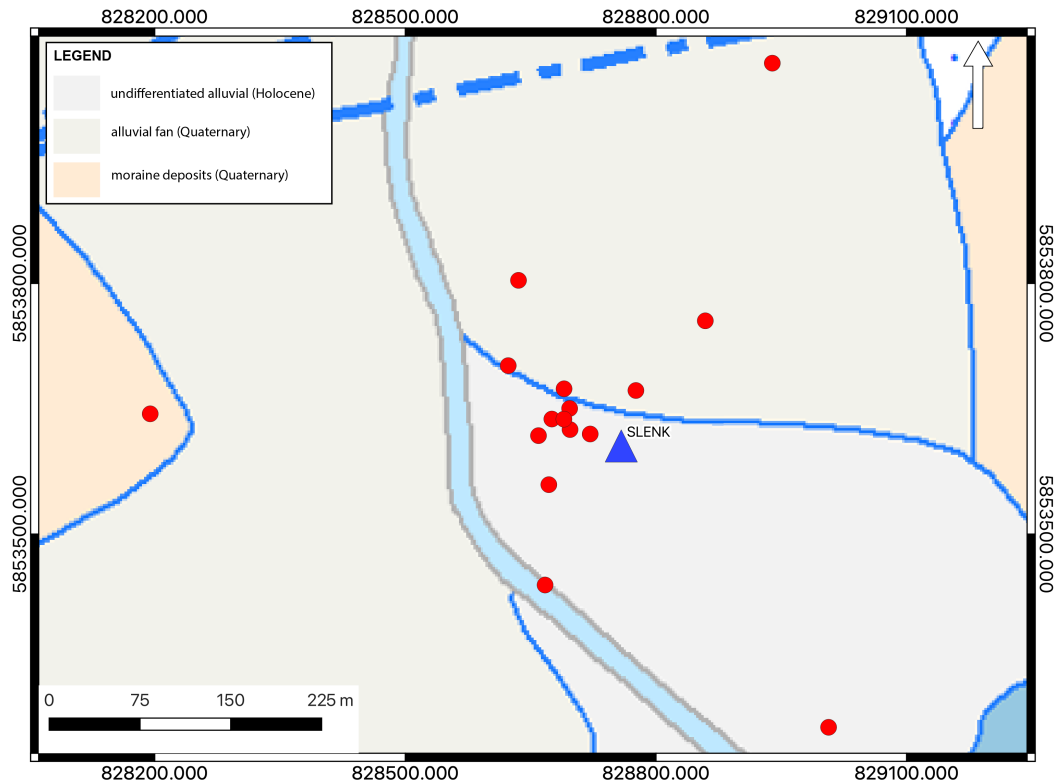
Figure 2: Geological map of the Lenk area. The stations of the passive array recordings are indicated by red triangles, whereas the position of the strong-motion station SLENK is shown by a blue triangle. Source: Federal Office of Topography.

The presence of alluvial deposits over the entire study area could be linked with the evolution of the river bed and the flood events involving the entire area. In order to reconstruct the path of the river *Simme* trough the village of Lenk over the last 170 years, we show the river bed evolution using aerial maps (*https://map.geo.admin.ch/*, *Source: Federal Office of Topography*). As shown in Fig. 3, the path of the main river changed between 1911 and 1912. In 1923, the path of a tributary was drastically modified and an additional channel with a water basin built.
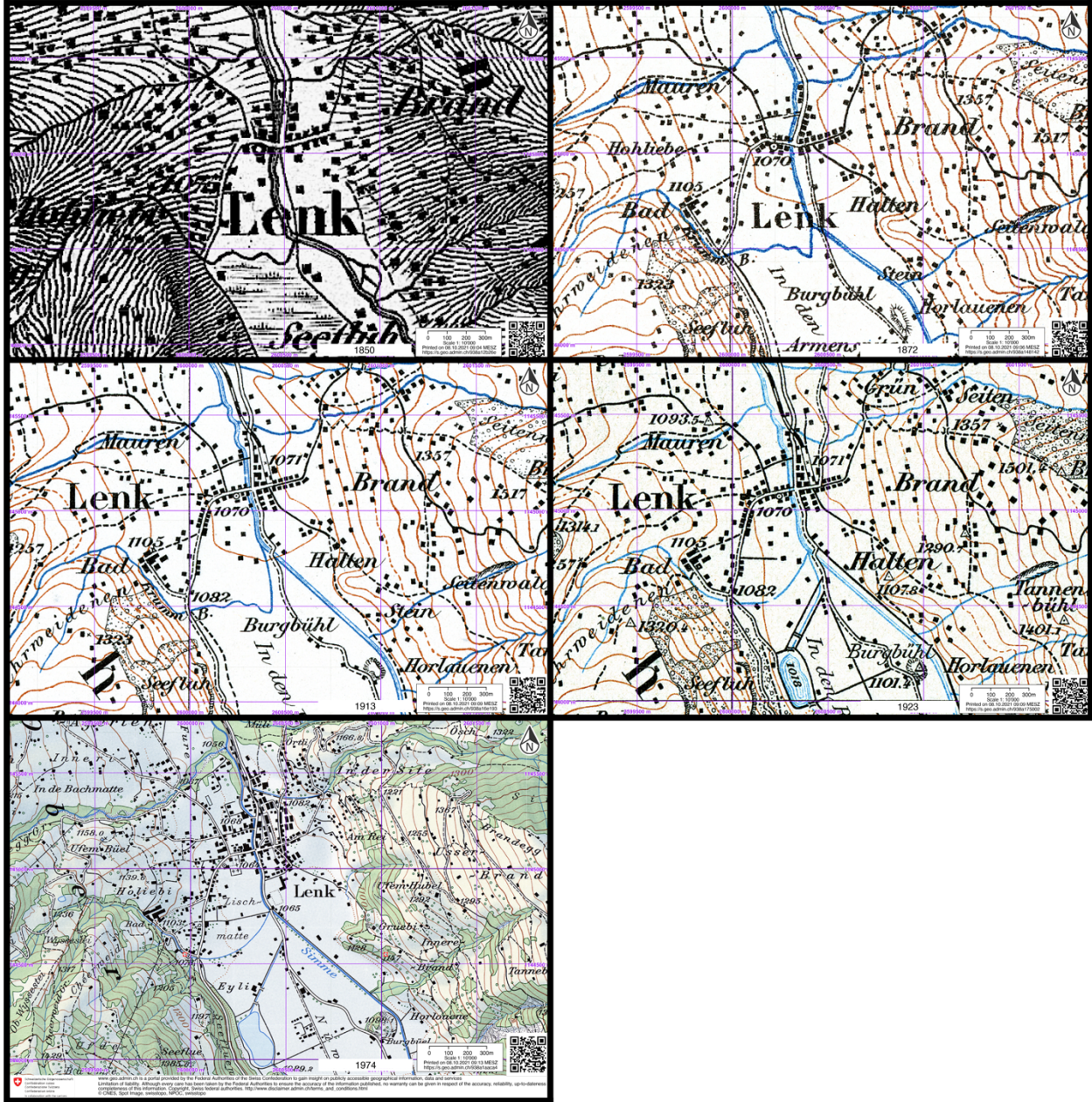
Figure 3: Aerial maps of the Lenk area in 1850, 1872, 1913, 1923 and 1974. Source: Federal Office of Topography.

3 Passive site characterization measurements

3.1 Data set

To characterize the underground structure around the seismic station, a passive seismic measurement and a H/V single point measurement at the location of station SLENK (SLENK1) were performed in October 2020.

A single array of 16 stations was installed (Fig. 5). The stations were planned to be located on five rings of different radii around a central station. The three stations of each ring were planned to be rotated 120 degrees one from the other for all rings with the exception of the fourth ring where the rotation angle changes between 111 and 131 degrees. The radii of the rings are 10, 25, 60, 140 and 340 meters. The array central station (LENK59) is located about 50 m in direction north-west from the station SLENK. On the original plan each ring was rotated with respect to the inner ring of 30, 57, 15 and 51 degrees. Unfortunately, due to an underground garage and of a small river crossing the village, we were forced to move two seismic stations to different locations (LENK44 and LENK49).

Each station consisted of a Lennartz 5s sensor connected to a Centaur digitizer, with the exception of four stations in the central part which had two sensors connected to the same digitizer. The station names of the array are composed of "LENK" followed by a two-digit number between 42 and 49, 52 and 59. The stations with numbers between 56 and 59 were connected to the second channel of digitizers between 46 and 49. The array recording time was 184 minutes (11040s). The station locations were measured by a differential GPS system (Leica Viva GS10) which was set up to measure with a precision better than 2.2 cm.

Figure 4: Seismic station installation example for the measurements in Lenk.
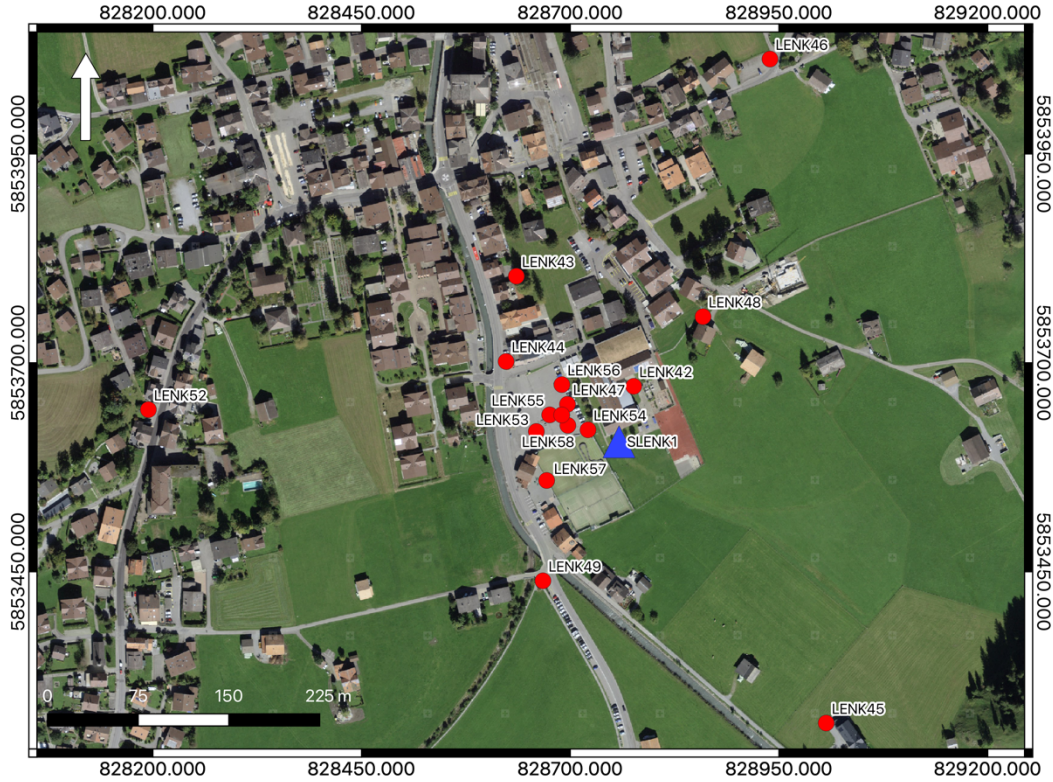
Figure 5: Layout of the array measurement in Lenk. The locations of the stations for the passive seismic measurement are indicated by the red dots. The blue triangle indicates the H/V point measured close to the seismic station site SLENK. Source: Federal Office of Topography.

3.2 H/V and RayDec ellipticity curves

Figure 6 shows the H/V and the RayDec ellipticity curves determined using the time-frequency analysis method (Fäh et al., 2009) and the RayDec technique (Hobiger et al., 2009) for all stations of the passive array and for the H/V point close to the permanent installation (SLENK1, see Fig. 5). Thirteen H/V curves show a wide peak with asymmetric flanks: a gentle flank on the left and a steep flank on the right. The fundamental H/V peak is located in a narrow frequency range between 1.4 and 2.0 Hz with amplitudes between 1.14 and 4. Above 4 Hz, to the right of the fundamental H/V peak, the curves show an almost flat trend with amplitude around 0.2 or 0.5. The 3 remaining H/V curves have different trends and the main peak are located at 1.15, 1.9 and 2.8 Hz.

The H/V curve measured close to the location of seismic station SLENK shows a gentle left flank and a steep right flank in agreement with all other curves and a wide peak at 1.54 Hz (dashed line). The subsurface underneath the investigated area is generally homogeneous as shown by the distribution of H/V fundamental peak frequencies (Fig. 7). Moving towards south and south-west, the frequency of the main H/V peak decreases (LENK45 and LENK49); vice versa towards east and north-east the frequencies increase (LENK46 and LENK48) meaning that the interface is getting shallower towards north.

The RayDec technique is meant to eliminate the contributions of other wave types than Rayleigh waves and give a better estimate of the ellipticity. The RayDec ellipticity curves for all stations of the array measurements are shown in Figure 6 (right plot). These show a pattern similar to the

curves obtained through the H/V analysis. While the trend is well represented for almost all ellipticity curves right of the fundamental H/V peak, the left flank appears a bit more confused with several wiggles. The dark green curve indicates the array central station, while the red curve shows the RayDec ellipticity measured close to station SLENK. This doesn't show a clear peak and its values increase towards lower frequencies.
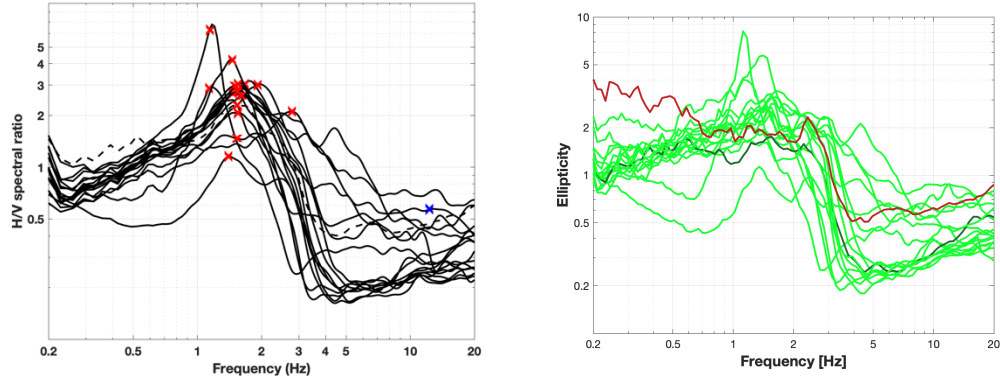
Figure 6: Left: H/V curves of the different stations of the array measurements in Lenk with picked fundamental frequency (red cross) and first higher mode (blue cross). Right: RayDec ellipticities for all stations of the array. The curve of LENK59, the array center, is highlighted in dark green, whereas the curve SLENK1, linked to the measurement nearby the station is represented using a dashed style (left plot) or highlighted in dark red (right plot).

Figure 7: Map showing the variation in frequency for the H/V fundamental peak over the area of Lenk. Source: Federal Office of Topography.

11

3.3 Polarization measurements

The polarization analysis was performed according to Burjánek et al. (2010) and Burjánek et al. (2012). The results for all stations of the array are similar. The ground motion is linear and horizontally polarized around the H/V peak at all sites (Fig. 8 – left plot). Most of the stations located in the center of the array and the station LENK49 shows a linear ground motion also between 5 and 8 Hz. For what concerns the directions of polarization we do not recognize any dominant direction (e.g. Fig. 8 – right column).

The results for SLENK59, the array center (see location in Fig. 5), and SLENK1 are shown in Fig. 8, respectively.
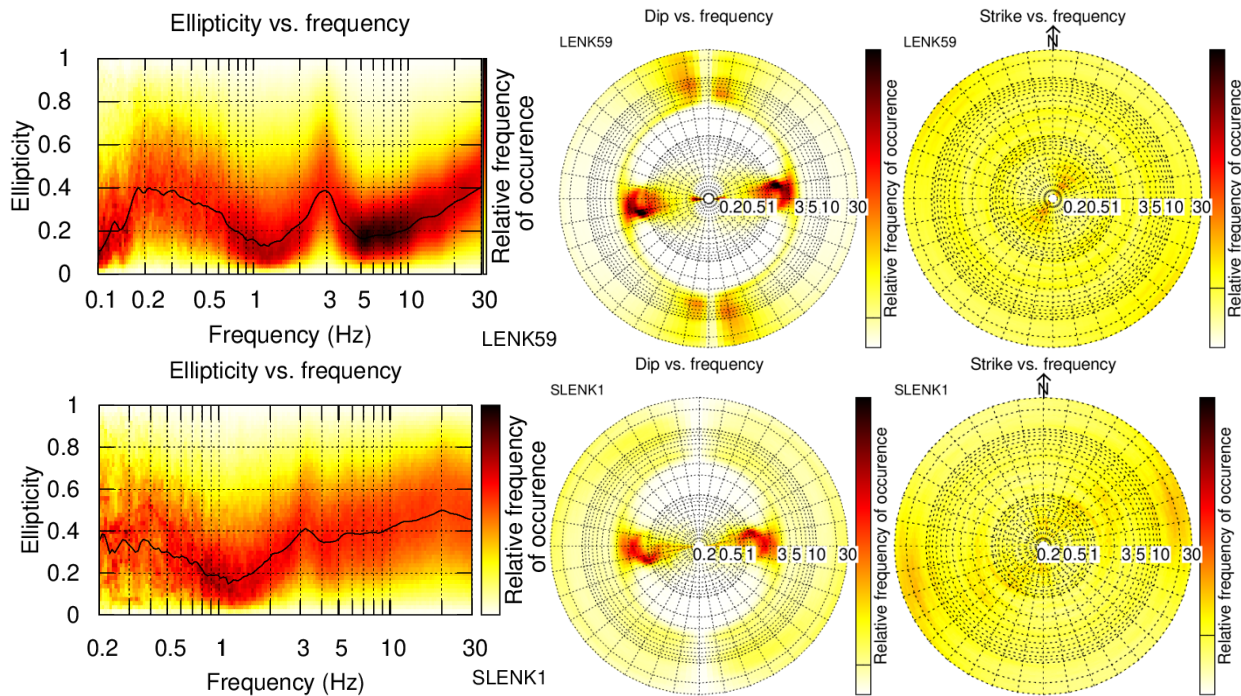

Figure 8: Polarization analysis of station SLENK59 (top line) and SLENK1 (bottom line).

3.4 3-component high-resolution FK

The results of the 3-component high-resolution FK analysis (Poggi and Fäh, 2010) are shown in Fig. 9. For Love waves, using the transverse component, three dispersion curves were picked between 1.20 and 14.55 Hz. A dispersion curve was also picked for the vertical component between 1.13 and 11.21 Hz. On the radial component, two short curves were picked between 1.28 and 3.29 Hz and between 2.91 and 5.43 Hz. Over the same frequency range as the dispersion curves picked using the vertical and the radial components, the ellipticity curves were picked (Fig. 9 – bottom line). Some similarity for the ellipticity curves, in terms of shape but not in terms of amplitude, can be seen at low frequencies between the curve picked for the vertical component (Fig. 9 – bottom line left) and the curve at lower velocity picked using the radial component (Fig. 9 – bottom line center).
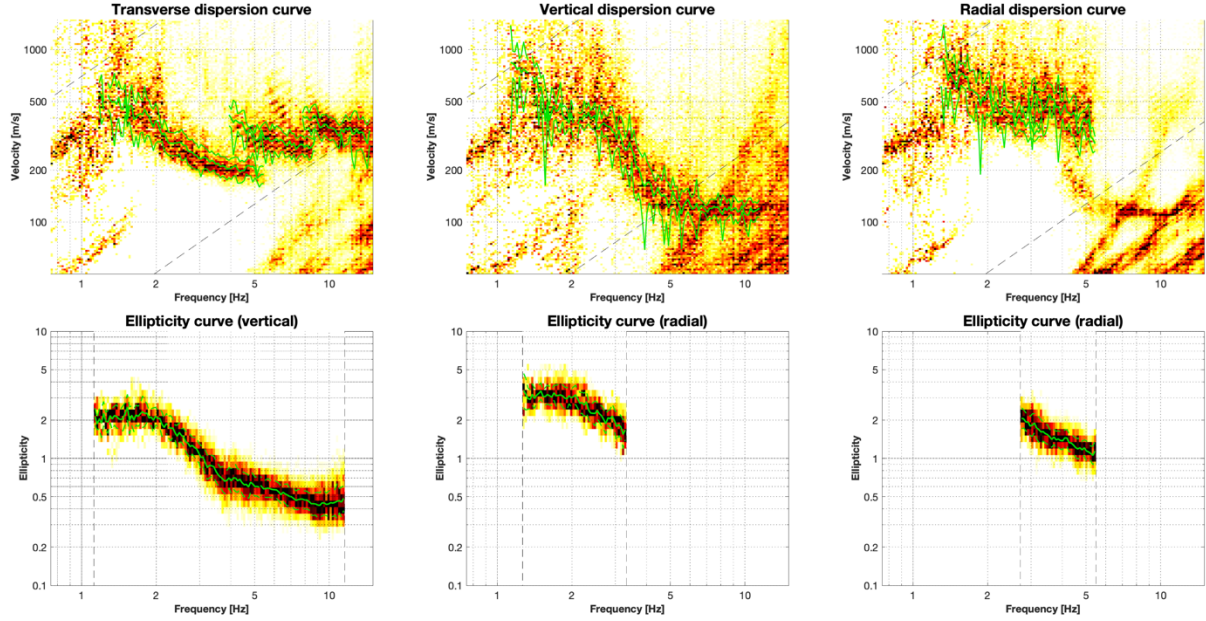
Figure 9: Top line: dispersion curves for the transverse (left), vertical (center) and radial (right) components obtained with the 3-component HRFK algorithm (Poggi and Fäh, 2010). Bottom line: ellipticity curves for the vertical component (left) and for the two ellipticity curves for the radial component (center and right). The dashed and dotted black lines are the array resolution limits. The solid and dashed green lines represent the data picking (central line) and the standard deviation (outer lines).

3.5 WaveDec

The results of the WaveDec (Maranò et al., 2012) processing are shown in Fig. 10. This technique estimates the properties of single or multiple waves simultaneously with a maximum likelihood approach. In order to get good results, the parameter γ must be tuned to modify the sharpness of the wave property estimation between purely maximum likelihood estimation and a Bayesian Information Criterion. Here, a value of $\gamma = 1$ was used, corresponding to a pure Bayesian Information Criterion estimation.

The picking of dispersion curves in WaveDec was performed in the wavenumber-frequency domain. The Love wave dispersion curve was continuously picked between 1.34 and 4.28 Hz, while the Rayleigh wave dispersion curve was picked between 1.36 and 4.78 Hz. The ellipticity angle picked for the Rayleigh wave dispersion curve is almost flat up to 2 Hz showing positive and negative values (+/- pi/2). Above 2 Hz, the ellipticity angle amplitude decreases, crosses below zero at about 3.5 Hz and remains constant up to 4.7 Hz. The frequency range between 2 and 3.5 Hz shows a prograde particle motion changing into retrograde up to 4.7 Hz. At lower frequencies, a retrograde particle motion is expected but the ellipticity angle curve is flat and the values are both positive and negative.
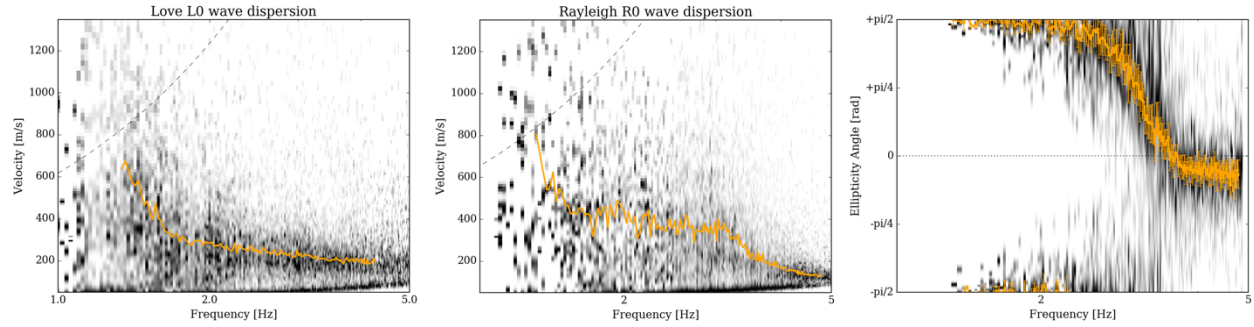
Figure 10: Dispersion curves for Love (left) and Rayleigh waves (center) and ellipticity angle curves for Rayleigh waves (right) as obtained with WaveDec (Maranò et al., 2012). The dashed black lines (top rows) represent the array resolution limits, the solid orange line indicates the picked curve and the vertical bars at each frequency show the standard deviation for the ellipticity angle curves.

3.6 Modified SPatial AutoCorrelation

The SPAC (Aki, 1957) curves of the vertical components have been calculated using the MSPAC (Bettig et al., 2001) technique implemented in geopsy. Rings with different radius ranges are defined and for all stations pairs with distances inside this radius range, the cross-correlation is calculated in different frequency ranges. These cross-correlation curves are averaged for all station pairs of the respective ring and give the SPAC curves. The rings are defined in such a way that at least three station pairs contribute and that their connecting vectors have a good directional coverage.

The SPAC Autocorrelation curves are shown in Fig. 11 for all selected rings. (central and right columns). The black points indicate the data values which contributed to the final dispersion curve estimation, which was picked using *spac2disp* of the geopsy package. One dispersion curve was picked for the Rayleigh wave between 1.21 and 5.53 Hz as shown by the dark gray curve in Fig. 11 (left).
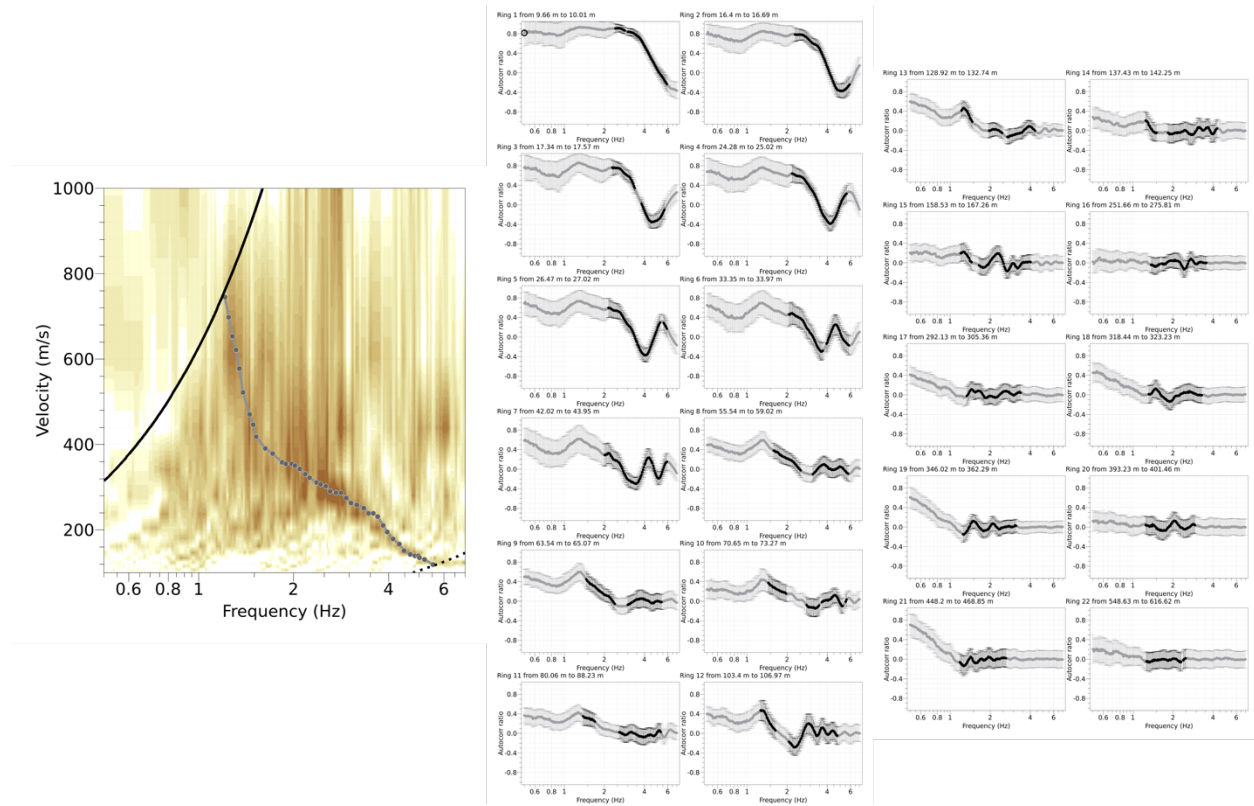
Figure 11: Rayleigh wave dispersion curve (left) obtained using spac2disp module of geopsy package and autocorrelation functions for all rings (center and right). The solid gray line represents the picked data; the black dashed and dotted lines indicate the array resolution limits.

3.7 Summary

Figure 12 gives an overview of the Love and Rayleigh wave dispersion curves (left and central plots, respectively) and of the Rayleigh wave ellipticity curves (right plot) determined using different approaches. For Love waves, using the results of 3C-HRFK technique, three branches of dispersion curves were picked at 1.36-4.90 Hz, 2.98-7.89 Hz and 7.80-14.55 Hz. Using WaveDec, one curve was picked between 1.34 and 4.28 Hz; this curve above 2 Hz overlaps with the curve at low velocity from 3C-HRFK. At lower frequencies, instead, the two curves diverge shaping an eye.

For the Rayleigh waves, all methods computed at least one curve. Using 3C-HRFK (vertical component) and WaveDec, an identical curve was picked between 1.13 and 4.91 Hz. At higher frequencies, up to 11.2 Hz, using the vertical component of 3C-HRFK, a flat curve with S-wave velocities of about 118 m/s was picked. The results of MSPAC show a curve between 1.21 and 5.54 Hz with velocities comparable with the other two curves but smoother shape. Finally, two curves were picked using the radial component of 3C-HRFK: one was picked between 1.28 and 3.29 Hz and it is close to all the other curves; the other is located between 2.91 and 5.93 Hz, at higher velocities.

The ellipticity curves retrieved using RayDec and 3C-HRFK are quite similar between 1 and 3 Hz. (Fig. 12 - right plot). A good fit up to 5 Hz is achieved for the RayDec curve computed using the central station and the ellipticity curve for the vertical component using 3C-HRFK technique. With

much higher ellipticity values and completely different shape, the ellipticity angle curve computed using WaveDec shows a broad peak at about 1.9-2 Hz followed by a narrow trough at about 3.65 Hz.
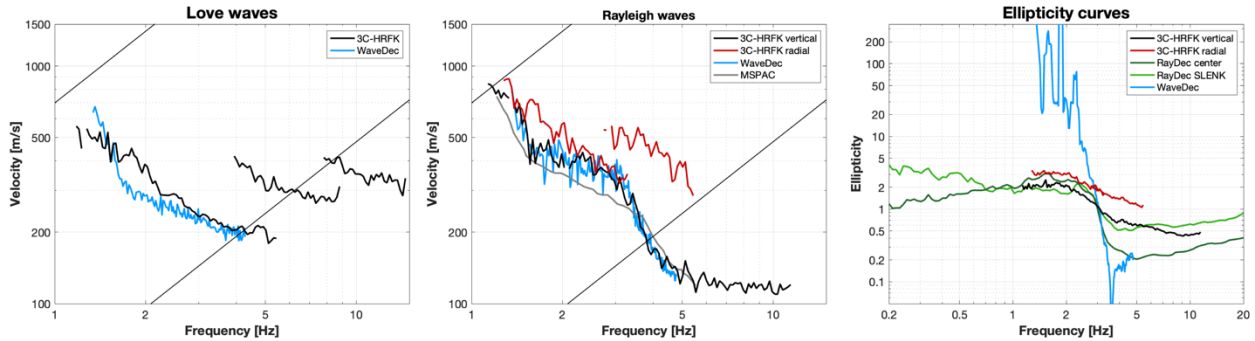

Figure 12: Comparison between the computed Love (left) and Rayleigh (center) wave dispersion curves and ellipticity curves (right).

4 Data inversion

4.1 Inversion targets

We performed several inversions using as much information as possible. The details of the inversion targets are indicated in Table 1 and the corresponding curves are shown in black in Fig. 13.

In the inversion process, we inverted two dispersion curves for the Love waves, one for the Rayleigh wave and one for the Rayleigh wave ellipticity curve. The Love wave dispersion curve at lower velocities was interpreted as fundamental mode, while the other as first higher mode; the curve for the Rayleigh waves was interpreted as fundamental mode. These curves were all picked using the results of 3C-HRFK technique. The ellipticity curve is the result of RayDec curve for the station SLENK59 (array center) at low and high frequencies and the ellipticity angle curve for the fundamental mode computed using WaveDec.
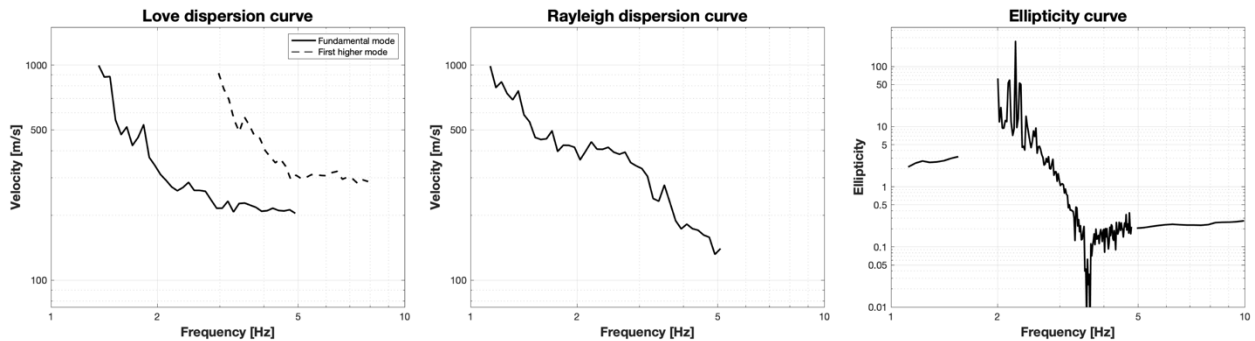

Figure 13: Overview of the dispersion curves (left and center) and ellipticity curve (right) used as target for the different inversions.

Table 1: List of the curves used as target in the inversion.

Method	Wave type	Mode	Curve type	Frequency range [Hz]
3C-HRFK	Love	fundamental	dispersion	1.2-5.4
3C-HRFK	Love	first	dispersion	3.3-8.8
3C-HRFK	Rayleigh	fundamental	dispersion	1.1-5.1
RayDec / WaveDec	Rayleigh	fundamental	ellipticity	1.1-10.0

4.2 Inversion parameterization

For the inversion, five different parameterizations were tested. The first four involve free values of thickness and velocities for the different layers, ranging from five to eleven layers over the half-space. The S- and P-wave velocities are allowed to range from 50 to 3500 m/s and from 100 to 7500 m/s, respectively. The deepest layer interfaces were allowed to range to a depth of 400 m for all parameterizations. The density was fixed to 2300 kg/m^3 for the bedrock layer; for the other layers a fix value, increasing with depth, was set between 2000 and 2200 kg/m^3.

The last parameterization had fixed layer thicknesses and consists of 20 layers over the half-space, with the deepest interface at 400 m depth. Equal ranges were defined for the P- and S-wave velocities and density.

4.3 Inversion results

We performed a total of 5 inversions with different parameterizations (see Table 2) using the Dinver routine (http://www.geopsy.org/). Each inversion run produced 280000 total models in order to assure a good convergence of the solution. The results of these inversions are shown in Figs 14 – 18.

Table 2: List of inversions

Inversion	Number of layers	Number of models	Minimum misfit
SLENK 5l	5	280000	0.447
SLENK 7l	7	280000	0.455
SLENK 9l	9	280000	0.462
SLENK 11l	11	280000	0.477
SLENK fix	20	280000	0.405

Figure 14: Inversion SLENK 5l. Top line: P-wave velocity profiles (left), S-wave velocity profiles (center) and Ellipticity angle (right). Bottom line: Dispersion curves for the fundamental mode of Rayleigh wave (left), for the fundamental mode of Love wave (center) and the first higher mode (right). The black dots indicate the data points used for the inversion, the black bars the standard deviation of the inverted curve, while the gray line shows the best-fitting model.
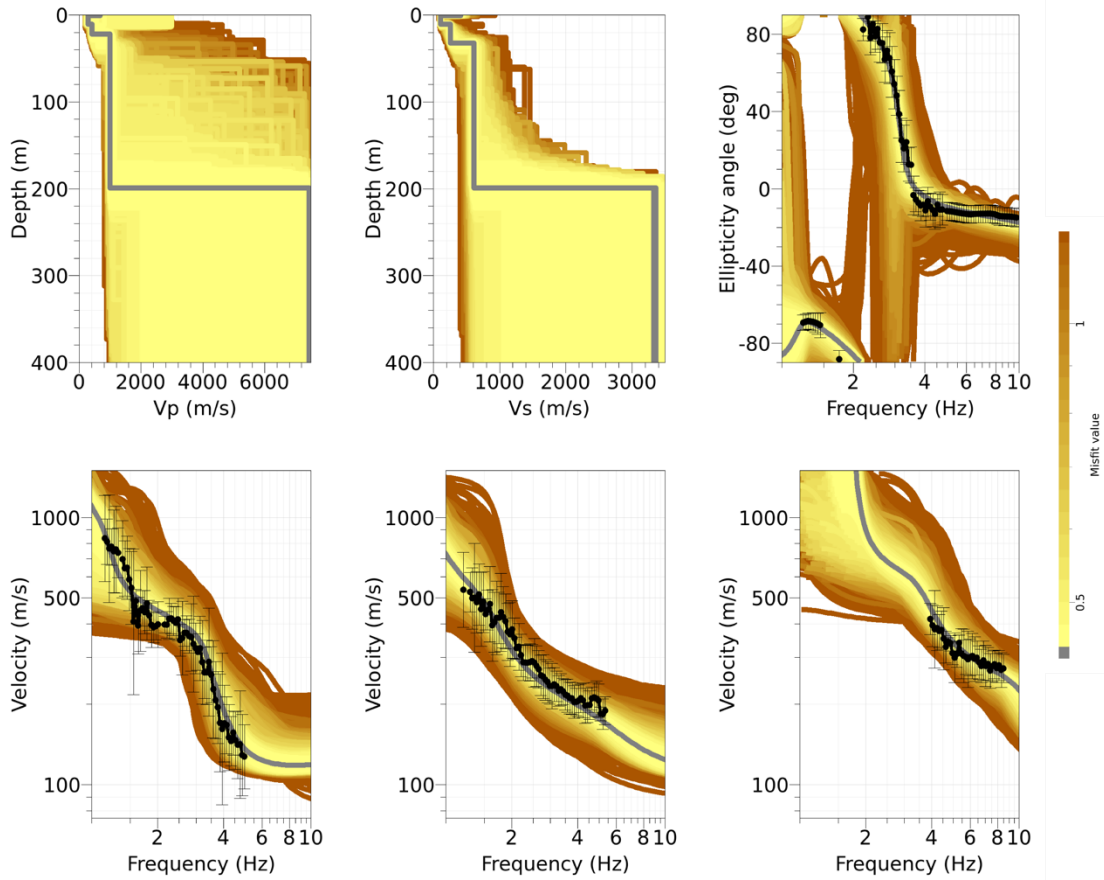
Figure 15: Inversion SLENK 7l. Top line: P-wave velocity profiles (left), S-wave velocity profiles (center) and Ellipticity angle (right). Bottom line: Dispersion curves for the fundamental mode of Rayleigh wave (left), for the fundamental mode of Love wave (center) and the first higher mode (right). The black dots indicate the data points used for the inversion, the black bars the standard deviation of the inverted curve, while the gray line shows the best-fitting model.
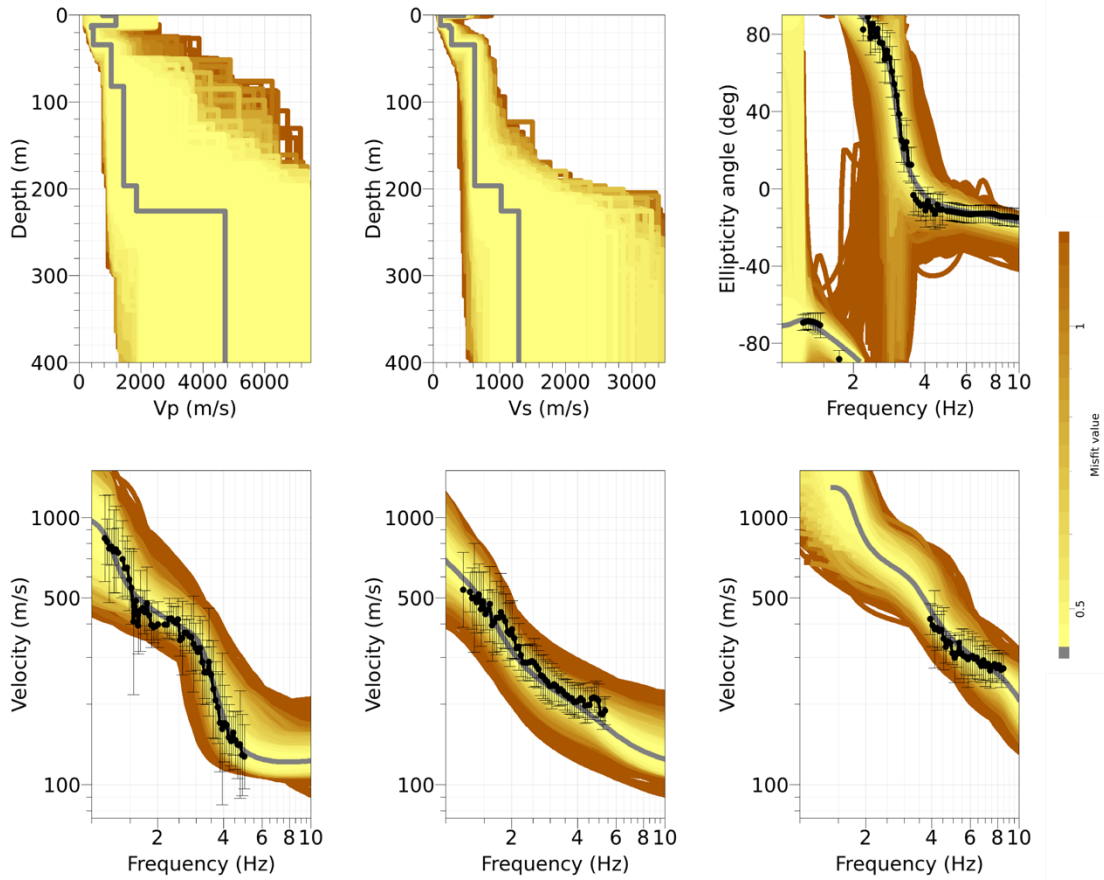
Figure 16: Inversion SLENK 9l. Top line: P-wave velocity profiles (left), S-wave velocity profiles (center) and Ellipticity angle (right). Bottom line: Dispersion curves for the fundamental mode of Rayleigh wave (left), for the fundamental mode of Love wave (center) and the first higher mode (right). The black dots indicate the data points used for the inversion, the black bars the standard deviation of the inverted curve, while the gray line shows the best-fitting model.
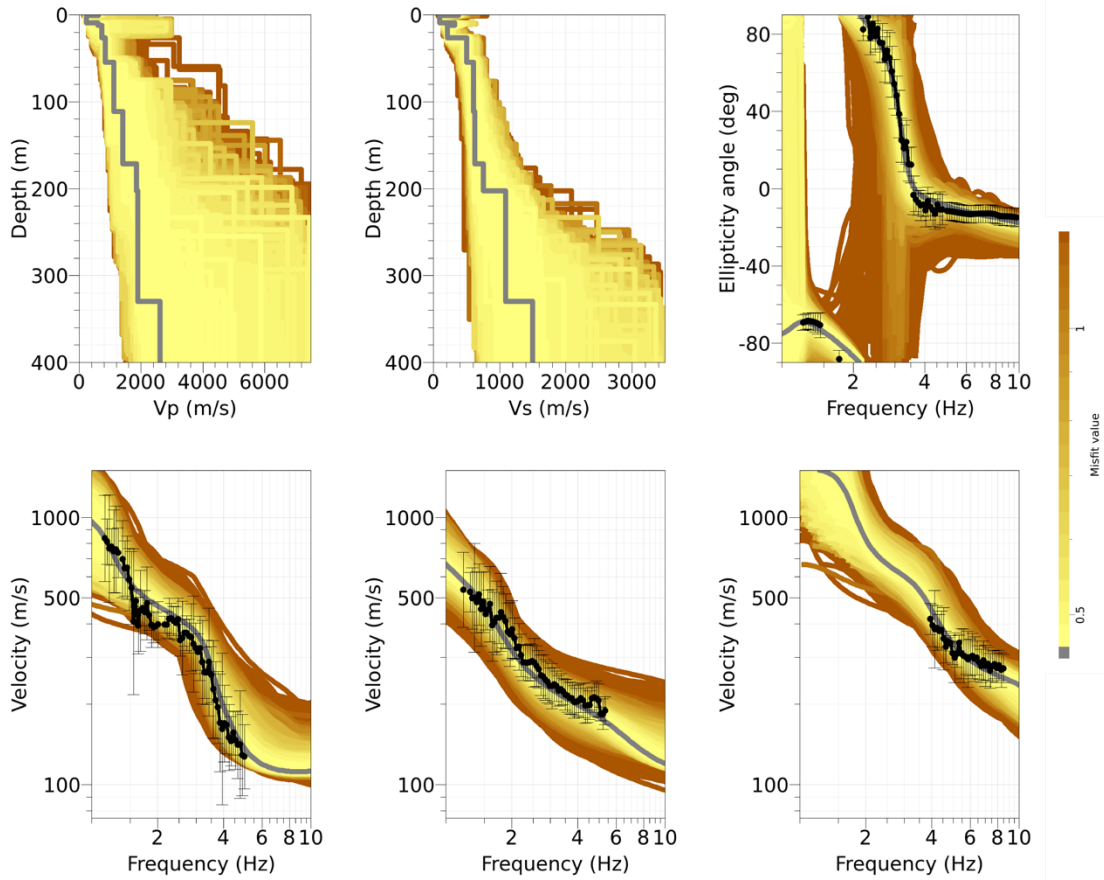
Figure 17: Inversion SLENK 11l. Top line: P-wave velocity profiles (left), S-wave velocity profiles (center) and Ellipticity angle (right). Bottom line: Dispersion curves for the fundamental mode of Rayleigh wave (left), for the fundamental mode of Love wave (center) and the first higher mode (right). The black dots indicate the data points used for the inversion, the black bars the standard deviation of the inverted curve, while the gray line shows the best-fitting model.
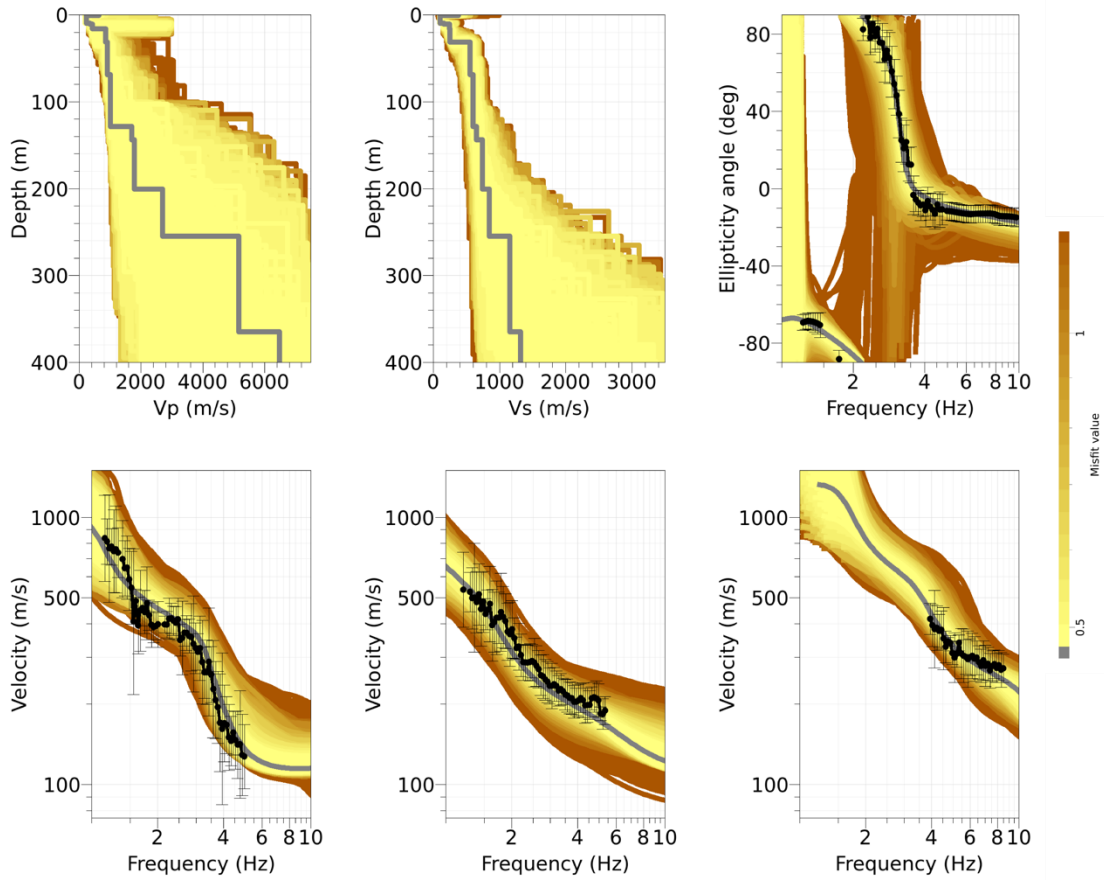
Figure 18: Inversion SLENK fix. Top line: P-wave velocity profiles (left), S-wave velocity profiles (center) and Ellipticity angle (right). Bottom line: Dispersion curves for the fundamental mode of Rayleigh wave (left), for the fundamental mode of Love wave (center) and the first higher mode (right). The black dots indicate the data points used for the inversion, the black bars the standard deviation of the inverted curve, while the gray line shows the best-fitting model.
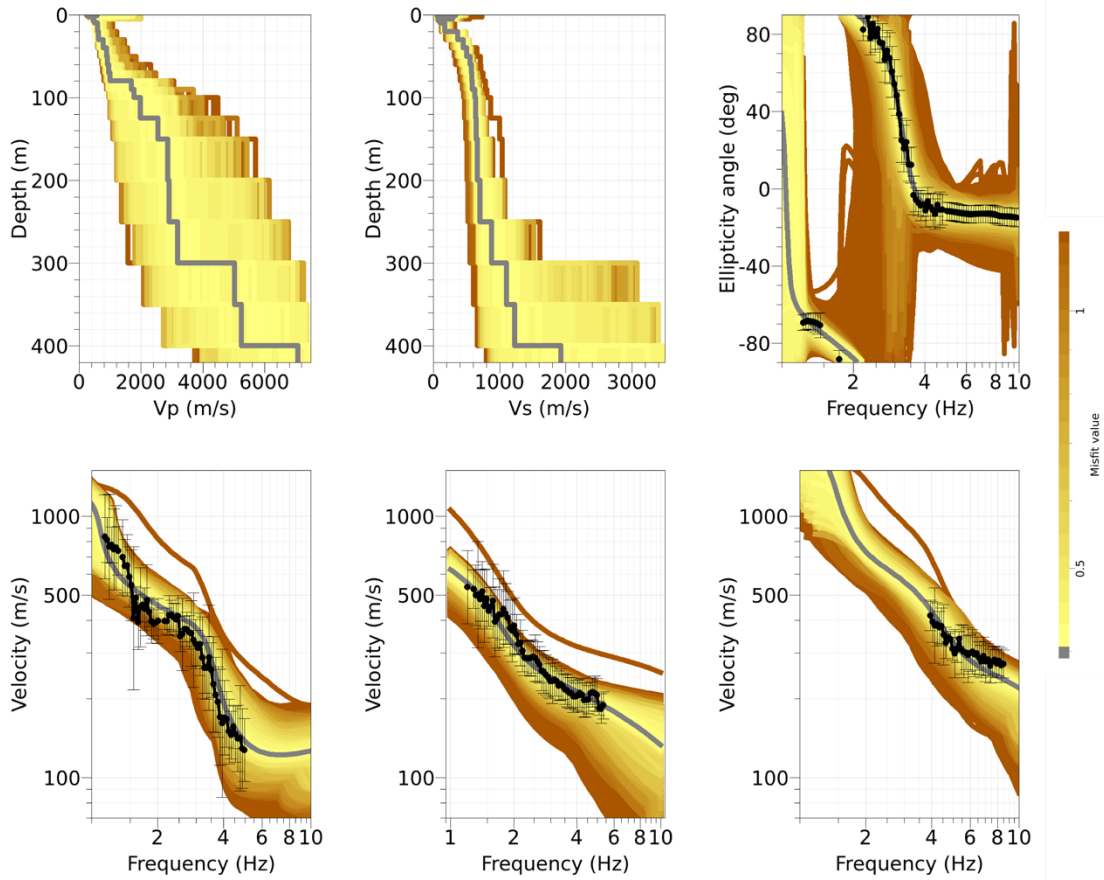
4.4 Discussion of the inversion results

The best-fitting models from each parametrization are shown in Fig. 19: S-wave velocity profiles down to 420 meters (left) and zoom into the first 30 meters (right).

To run the final inversion and estimate the velocity profiles for the investigated site, some initial tests were performed to define the features of the initial parametrization. Based on our preliminary results, we allowed a low-velocity zone to occur in the first 15 meters.

In the first 30 meters, all velocity profiles show one thin layer of 1 meter thickness with S-wave velocities between 380 and 465 m/s overlying a low velocity zone of about 107 m/s occurring down to 10-12 meters. Three interfaces are identified by all velocity profiles: at about 11, 32 and 200 meters. The S-wave velocities of the first and second interfaces are around 256 and 612 m/s, respectively. The third interface has S-wave velocities from 844 m/s (*SLENK11l*) to 3333 m/s (*SLENK5l*). The strong velocity contrast shown by the best model of *SLENK5l* corresponds to the transition with the half-space and its shallow investigated depth compared to the results of all the other models proves the low resolution of this model. A not unique half-space with similar S-wave velocities was identified by all models at 226 m (*SLENK7l*), 330 m (*SLENK9l*) and 365 m (*SLENK11l*).

The velocity profile obtained using the fix layers parametrization (*SLENK fix*) shows a constant increase of velocity with depth. The transition to the half-space shows an S-wave velocity increase from about 1232 m/s to 1928 m/s. Several interfaces of this profile are in agreement with the velocity contrasts found by the other velocity profiles (e.g. about 10, 30, 200, 250 m, etc.). In the shallow layers, instead of an unique low-velocity zone as shown by the other best models, the velocity profile *SLENK fix* shows two low-velocity zones starting at 1 and 5 m.

The velocity profiles resulting from the different inversions have V_{S30} between 171.86 and 177.45 m/s, with an average value of 175.57 ± 2.18 m/s.
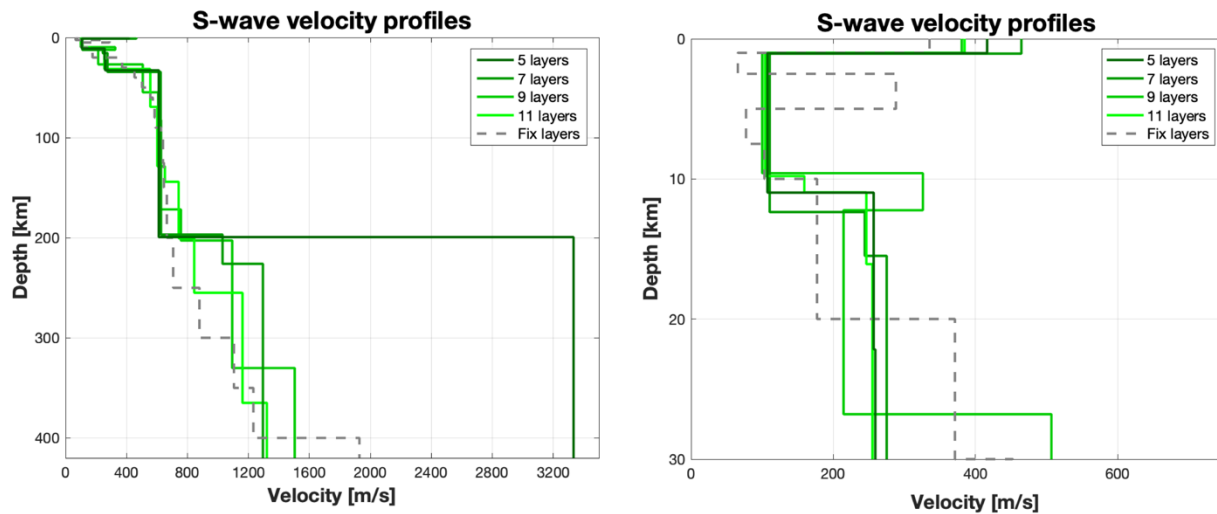

Figure 19: Overview of the best shear-wave velocity profiles of the different inversions (left) and zoom on the upper 30 m of the inversion profiles.

5 Further results from the inverted profiles

5.1 SH transfer function

In Figure 20, the average theoretical shear-wave transfer function from the best velocity profiles and the empirical amplification at station SLENK are shown. For the investigated site, the average theoretical shear-wave transfer function predicts a wide peak between 1.1 and 5.62 Hz with an amplification up to 7.9 followed by a second and narrower peak at about 7.66 Hz. To the right of the peak, the amplification decreases down to 1 at 28 Hz. The empirical function computed using the earthquake recordings at station SLENK shows a wide peak at low frequency and constant amplification values around 4-5 up to 20 Hz. The present (28.06.2021) empirical amplification has a maximum of 40 earthquakes between 1.97 and 6.71 Hz decreasing to 0 above 28.4 Hz. Even if the number of recorded earthquakes is low, the wide peak at low frequency is well represented in terms of shape and amplification values.
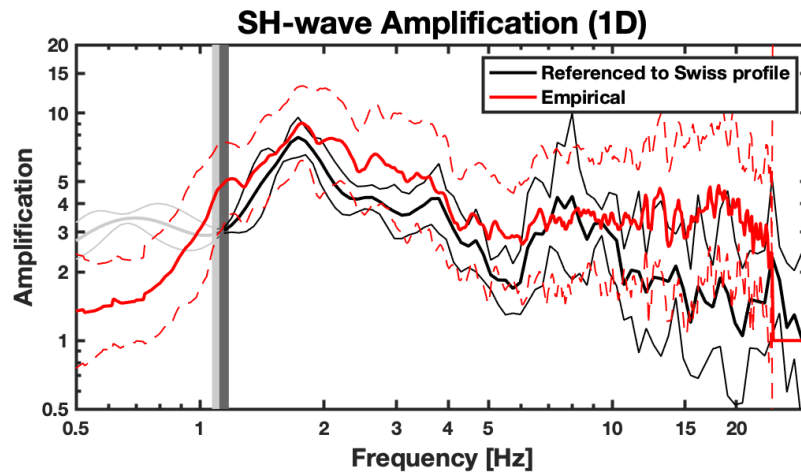

Figure 20: Modeled amplification function and standard deviation (black lines). Red curves represent the empirical amplification (solid line) and its standard deviation (dashed lines) function at the station SLENK.

5.2 Quarter-wavelength representation

The quarter-wavelength velocity approach (Joyner et al., 1981) provides, for a given frequency, the average velocity at a depth corresponding to 1/4 of the wavelength of interest (Fig. 21). The results using this proxy, considering frequency limits of the experimental data between 1.1 to 8.8 Hz for the dispersion curves and between 1.1 and 10.0 Hz for the ellipticity curves, is well constrained down to 30 m and below. The quarter wavelength impedance-contrast introduced by Poggi et al. (2012) is also displayed in the figure. It corresponds to the ratio between two quarter-wavelength average velocities, respectively from the top and the bottom part of the velocity profile, at a given frequency.
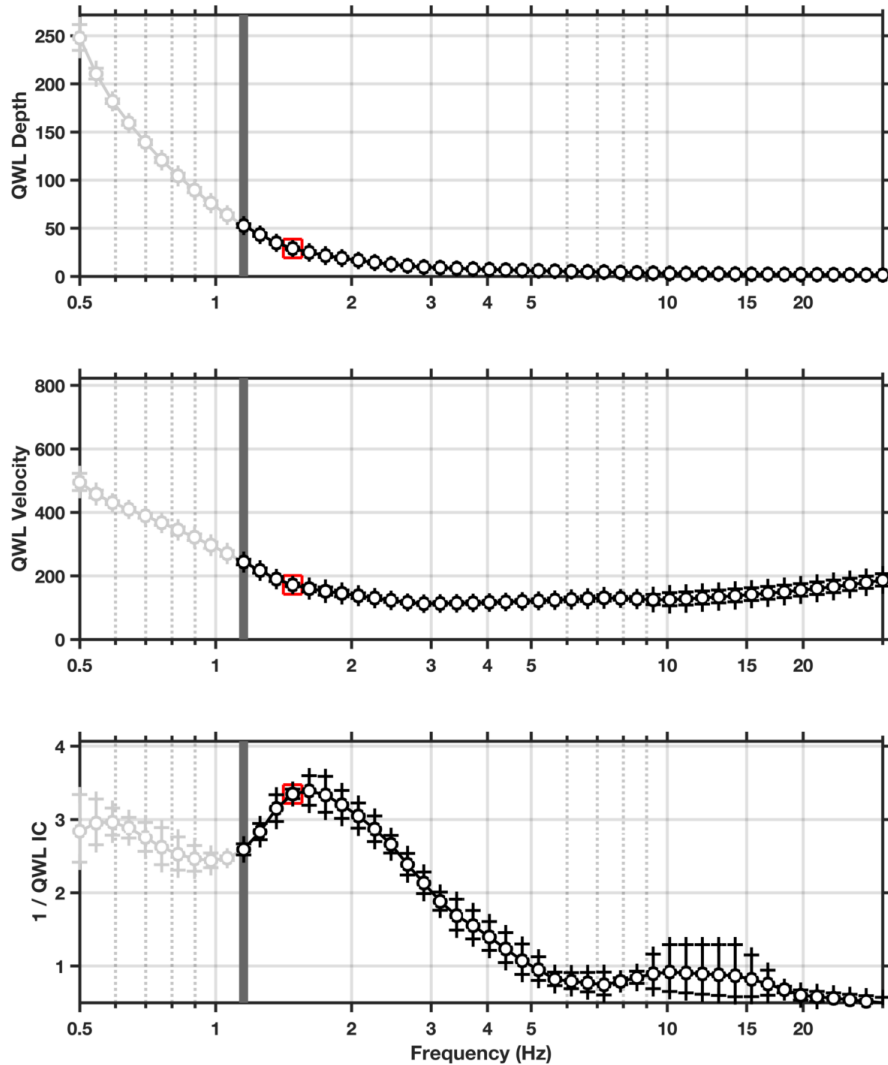
Figure 21: Quarter wavelength representation of the velocity profiles for the best models of the inversions (top: depth, center: velocity, bottom: impedance contrast). The grey light bar shows ellipticity lower frequency value, dark grey bar indicates lower frequency value obtained with dispersion curves and red square corresponds to f_{30} (frequency related to the depth of 30 m).

6 Discussion and conclusions

The passive array measurement performed in Lenk in October 2020 allowed the investigation of the subsurface underneath the station SLENK.

The H/V analysis pointed out that most of the study area consists in a homogeneous layer getting shallower towards north-east and deeper towards south and south-east. Most of the curves in the center of the study area show an asymmetric peak at about 1.4-2.0 Hz followed by a wide trough (Fig. 6 – left plot).

The inversion of the fundamental mode of Rayleigh waves, the fundamental and the first higher modes of Love waves and the fundamental mode of Rayleigh wave ellipticity curve yields to the estimation of P- and S-wave velocity profiles investigating the subsurface down to about 400 m. All velocity profiles show one shallow layers of 1 m thickness followed by a low-velocity zone down to 10-12 meters. Below the low velocity zone, three interfaces are identified by all velocity profiles at about 11, 32 and 200 meters. The 5 layers profile, due to its low resolution, is not able to represent the deep subsurface and locates the half-space at 200 meters with S-wave velocities up to about 3333 m/s. The other models locate the bedrock at 226 m (*SLENK7l*), 330 m (*SLENK9l*) and 365 m (*SLENK11l*) with an average S-wave velocity of about 1200 m/s.

The velocity profile obtained using the fix layers parametrization *(SLENK fix)* shows a gradual increase in velocity without strong interfaces with the exception of the transition to the half-space where the S-wave velocity increases from 1232 m/s to 1928 m/s.

The V_{S30} value of the site is determined as 175.57 m/s, corresponding to soil class D in EC8 and in SIA261 classifications.

The comparison of theoretical shear-wave transfer function and the empirical curve recorded at the seismic station SLENK show a quite good agreement between 0.75 and 5.62 Hz where a wide peak with an amplification of about 7.9 occurs. At higher frequencies, the empirical function is almost flat, while the theoretical shear-wave transfer function shows a descending trend up to 28 Hz with a secondary peak at about 7.66 Hz.

References

Burjánek, J., Gassner-Stamm, G., Poggi, V., Moore, J. R., and Fäh, D. (2010). Ambient vibration analysis of an unstable mountain slope. Geophys. J. Int., 180:820–828.

Burjánek, J., Moore, J. R., Molina, F. X. Y., and Fäh, D. (2012). Instrumental evidence of normal mode rock slope vibration. Geophys. J. Int., 188:559–569.

Fäh, D., Gardini, D., et al. (2003). Earthquake Cataloque of Switzerland (ECOS) and the related macroseismic database. Eclogae geol. Helv. 96.

Fäh, D., Wathelet, M., Kristekova, M., Havenith, H., Endrun, B., Stamm, G., Poggi, V., Burjanek, J., and Cornou, C. (2009). Using ellipticity information for site characterisation. NERIES deliverable JRA4 D4, available at http://www.neries-eu.org.

Fritsche, S., Fäh, D., Gisler, M., and Giardini, D. (2006). Reconstructing the damage field of the 1855 earthquake inSwitzerland: historical investigations on a well-documented event Geophys. J. Int. (2006)166, 719–731

Hobiger, M., Bard, P.-Y., Cornou, C., and Le Bihan, N. (2009). Single station determination of Rayleigh wave ellipticity by using the random decrement technique (RayDec). Geophys. Res. Lett., 36.

Maranò, S., Reller, C., Loeliger, H.-A., and Fäh, D. (2012). Seismic waves estimation and wavefield decomposition: Application to ambient vibrations. Geophys. J. Int., 191:175–188.

Poggi, V. and Fäh, D. (2010). Estimating Rayleigh wave particle motion from three component array analysis of ambient vibrations. Geophys. J. Int., 180:251–267.

Poggi, V., Edwards, B., and Fäh, D. (2010). Characterizing the Vertical-to-Horizontal Ratio of Ground Motion at Soft-Sediment Sites. Bulletin of the Seismological Society of America, 102(6): 2741 2756.